Dislocation Contrast from Phonon-Scattered Electrons in Weak-Beam Images

By Arne Melander and Rolf Sandström

Department of Theoretical Physics, Royal Institute of Technology, S-100 44 Stockholm 70, Sweden

A theory for the contrast from phonon-scattered electrons is presented. In this theory single-phonon scattering is taken into account. The influence of the strain field of the crystal defect on the electrons which have been scattered by phonons is considered dynamically. The dislocation contrast in the thermal diffuse intensity is calculated under weak-beam conditions at 100 kV and 1MV. It is shown that the thermal diffuse and elastic intensities are comparable in magnitude for foil thicknesses of the order of the mean free path for electron–phonon scattering. The thermal diffuse intensity has a minimum close to the position of the dislocation. The dependence of the visibility in weak-beam images on the foil thickness, the accelerating voltage, the aperture radius and the temperature is discussed. The diffuse intensity from contaminating carbon layers has been estimated.

1. Introduction

In conventional contrast calculations phonon scattering is only taken into account in the absorption parameters. The phonon scattering involves large angles and a large proportion of the electrons are scattered outside the aperture and do not contribute to the image. Consequently under strong-beam conditions, if the foil thickness is not much larger than the mean free path for phonon scattering, the thermal diffuse intensity is small compared to the elastic intensity. If, however, the elastic intensity is low, as in weak-beam images, the intensity from electrons scattered by phonons into the aperture may give a significant contribution to the intensity.

The thermal diffuse intensity in perfect crystals has been calculated, for example, by Takagi (1958) and Gjønnes (1966) in order to study Kikuchi patterns. These authors took single-phonon scattering into account. The influence of multiple scattering has been investigated by Høier (1972).

The contrast from phonon-scattered electrons has been studied for perfect wedge-shaped crystals by Castaing *et al.* (1967). With the crystal oriented close to a low-order Bragg position a weak depth oscillation was observed in the thermal diffuse intensity. Natta (1968) used first-order perturbation theory to show that these oscillations were caused by the simultaneous phonon scattering of two Bloch waves. The influence of a stacking fault on the diffuse intensity has been investigated by Kamiya & Nakai (1971). They evaluated the transition probabilities for phonon scattering in order to obtain a qualitative explanation of the experimental results.

In the present paper the influence of the thermal diffuse intensity on the dislocation contrast under weak-beam conditions will be investigated. In § 2 and the Appendix a theory for the contrast of the thermal diffuse intensity is presented. Most of the diffuse intensity comes from scattering between a few Bloch waves. This is analysed in § 3. An approximate ana-

lytical expression for the thermal diffuse intensity is derived in § 4. The results of the contrast calculations of dislocations are presented in § 5. In § 6 the difference in contrast from dislocations close to the top and bottom foil surfaces, a so-called top–bottom effect, is discussed. How the thermal diffuse intensity depends on the foil thickness and aperture size is considered in § 7. The diffuse intensity from contaminating layers is estimated and its magnitude is compared with the magnitude of the thermal diffuse intensity. Finally in § 8, the variations of the visibility with accelerating voltage, foil thickness, aperture radius and temperature are discussed.

2. Contrast theory

Thermal diffuse intensity can be calculated using either the deformable ion model (DIM) or the rigid ion model (RIM) (Takagi, 1958). The main difference between these models is that DIM but not RIM gives zero matrix elements for scattering in the first Brillouin zone. In the weak-beam case this implies that the transition probabilities for intraband scattering are negligible. Actual calculations show, however, that the intensity contribution from the intraband processes can be neglected in RIM also compared to the interband processes. Thus the differences between the two models have a small influence on the results under weak-beam conditions. In this paper DIM has been used because it is somewhat simpler to handle. The derivation of the equations for the Bloch-wave amplitudes of the phonon-scattered electrons is presented in the Appendix. The result for phonon annihilation is

$$\frac{\mathrm{d}}{\mathrm{d}z}\,\varphi(\mathbf{k}^l_{p-},z)=2\pi i\sum_{gj}C^{l*}_{g}\left(\mathbf{g}\cdot\frac{\mathrm{d}\mathbf{R}}{\mathrm{d}z}\right)C^{j}_{g}$$

$$\times\exp\left[2\pi i(\mathbf{k}^j_{p-}-\mathbf{k}^l_{p-})_z\cdot z\right]\varphi(\mathbf{k}^j_{p-},z)$$

$$+2\pi^2\sum_{ghi}C^{l*}_{h}\frac{1}{\zeta_{h-g}}C^{i}_{g}[\mathbf{\varepsilon}_{q\lambda}\cdot(\mathbf{h}-\mathbf{g})]\left[\frac{\hbar n^0_{q\lambda}}{2NM\omega_{q\lambda}}\right]^{1/2}$$

$$\times\exp\left[2\pi i(\mathbf{k}^i_0+\mathbf{q}-\mathbf{k}^l_{p-})_z\cdot z\right]\varphi(\mathbf{k}^i_0,z)\,. \tag{1}$$

$\varphi(\mathbf{k}_{p-}^{l}, z)$ is the amplitude at depth z and $C_{\mathbf{g}}^{l}$ the coefficient of the Bloch wave with wavevector $\mathbf{k}_{p-}^{l}$ (p^{-} indicates phonon annihilation). The initially excited Bloch waves have the wave vectors $\mathbf{k}_{0}^{l}$. $\xi_{\mathbf{g}}$ is the two-beam extinction distance for the reciprocal-lattice vector $\mathbf{g}$. The lattice strains are given by $\mathbf{R}(\mathbf{r})$. The crystal contains N atoms of mass M, $\varepsilon_{\mathbf{q}\lambda}$ is the polarization vector, $\omega_{\mathbf{q}\lambda}$ the angular frequency and $n_{\mathbf{q}\lambda}^{0}$ the occupation number of the phonon mode $(\mathbf{q}, \lambda)$. The first term on the right-hand side takes into account the elastic scattering between the electrons which have been scattered by phonons. It has the same form as the expression for elastic scattering in the conventional many-beam theory (see e.g. Cockayne, 1972). The second term describes the phonon scattering from the primarily excited Bloch waves. It is equivalent to the corresponding term for plasmon scattering derived by Howie (1963).
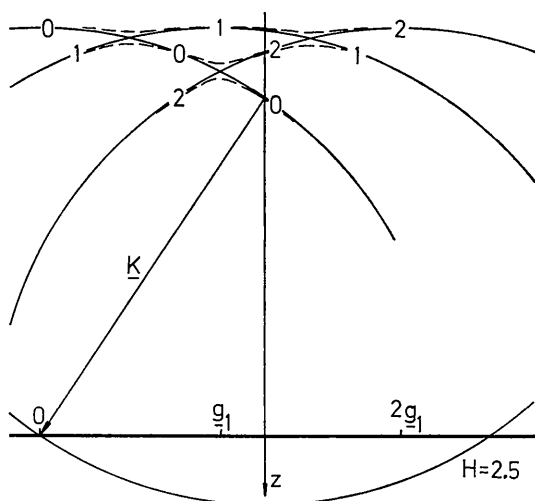

Fig. 1. Dispersion surfaces at 100 kV illustrating the numbering of the Bloch waves.
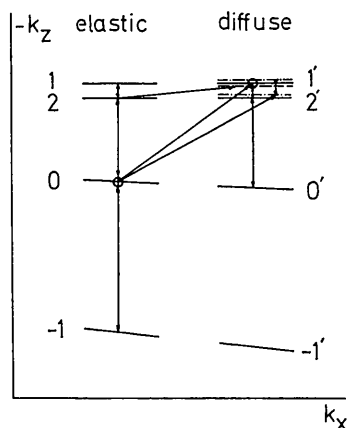

Fig. 2. Dispersion surfaces under weak-beam conditions at 100 kV ($H < 3$). The figure is not to scale.

The thermal diffuse intensity contributing to the weak-beam image from the reflexion $\mathbf{g}$ is obtained by summing over all phonon processes which allow the electrons to pass through the aperture. Electrons scattered by different phonons have different energy and cannot interfere coherently and consequently their intensities rather than their amplitudes have to be added. The intensity around the reflexion $\mathbf{g}$ can be written

$$I_{\mathbf{g}}^{ph}(t) = \sum_{\mathbf{q}\lambda l} \{| \sum_{l} \varphi(\mathbf{k}_{p-}^{l}, t) C_{\mathbf{g}}^{l} \exp [2\pi i(\mathbf{k}_{p-}^{l})_{z} t]|^{2}$$
$$+ | \sum_{l} \varphi(\mathbf{k}_{p+}^{l}, t) C_{\mathbf{g}}^{l} \exp [2\pi i(\mathbf{k}_{p+}^{l})_{z} t]|^{2} \}, \quad (2)$$

where the two terms take into account phonon annihilation and creation respectively. t is the foil thickness. In the summation over l only Bloch waves representing electrons which have been scattered by the same phonon should be included (cf. the discussion of Fig. 2). For every primary Bloch wave i the summation of phonon wavevectors $\mathbf{q}$ is restricted to those components in the plane of the foil which are inside the aperture. Since $\mathbf{q}$ is restricted to the first Brillouin zone, (2) is only valid for apertures entirely inside the zone.

In the formulae (1) and (2) only single-phonon scattering has been taken into account. By introducing absorption coefficients for phonon scattering also processes where the phonon-scattered electrons are scattered a second time out of the aperture are considered. Processes where the electrons have first been thermally scattered somewhere outside the aperture and then scattered back into the aperture are neglected. The importance of such processes increases with increasing foil thickness and our description cannot be expected to be valid for foil thicknesses much greater than the mean free path for phonon scattering. The influence of electronic excitations on the diffuse intensity has been neglected throughout the present article.

3. Weak-beam contrast

The phonon-scattered intensity has been calculated at 100 kV and 1 MV. The situation at 100 kV is illustrated in Fig. 1. The crystal is oriented so that the Ewald sphere intersects the systematic row at Hg_{1} where g_{1} is the first-order reciprocal-lattice vector in the systematic row, such that $H > 0$. The weak beam $+g_{1}$ is studied. The Bloch waves are numbered so that the plane wave $\exp [2\pi i(\mathbf{k}^{n} + n\mathbf{g}_{1}) \cdot \mathbf{r}]$, represented by a circle in Fig. 1, contributes the most to Bloch wave n indicated by a broken line in Fig. 1 (cf. Cockayne, 1972).

In the calculations a four-beam approximation has been used. On the left-hand side of Fig. 2 the dispersion surfaces of the elastically scattered electrons are shown. These primary states are connected to the phonon-scattered states by phonon wave vectors. The diffusely scattered states are denoted by primed numbers. The different dashed lines indicate that electrons

which are scattered by different phonons do not interfere coherently. The most important phonon-scattering processes are shown in the figure. The direct process 0 to 1' is dominating since the incident electron gives the largest contribution to Bloch wave 0 and Bloch wave 1' contributes the most to the g_1 image. The importance of the other scattering processes can be estimated by evaluating the corresponding terms of equation (1).

An excitation error $s_{g_1} \simeq 0.02$ Å^{-1} for a 220 row corresponds in most metals to $H \simeq 3$, thus making the elastic scattering from the dislocation between Bloch waves 1' and 2' dynamical. If the elastic scattering between the diffuse states is strong the thermal diffuse intensity accepted by the aperture is sensitive to the position of the Kikuchi lines. For H values close to three at 100 kV the $-g_1$ edge of the central Kikuchi band is close to the g_1 spot and influences the diffuse intensity in the g_1 image. In the four-beam approximation this is taken into account.

At 1 MV the situation is slightly different as shown in Fig. 3. Since the curvature of the Ewald sphere decreases with increasing voltage a larger H value is required at 1 MV to obtain the same excitation error than at 100 kV. At 1 MV the $-g_1$ beam ($H>0$) is mostly used to form the weak-beam image. In this case the elastic scattering from the defect between the Bloch waves is weak and principally kinematical in character and the influence of the Kikuchi lines on the $-g_1$ image is much smaller that at 100 kV.

To obtain the phonon-scattered intensity accepted by the aperture we sum over the phonon wave vectors as indicated in (2). This sum includes processes where the wave vector is not conserved in the z direction. Such processes have a strong influence on the diffuse contrast, as we shall see. It follows from periodic boundary conditions that the z component of the phonon wave vectors q_z takes values of the form

$$q_z = \frac{n}{t} \, ,$$

where n is an integer. The summations over q_z should be performed over these values. For every q_z the Bloch-wave amplitudes in (2) are assumed to be constant over the aperture (see Appendix). The summation over $\mathbf{q}$ in the plane of the foil can then be reduced to a one-dimensional integral which is performed numerically. For aperture sizes within the first Brillouin zone, centred around the reciprocal-lattice vectors, this is a good approximation at 1 MV because of the large H values used. At lower voltages smaller H values are required and the approximation is somewhat less satisfactory for large aperture radii.

4. Long-range contrast

In this section an analytical estimate of the diffuse intensity is made which is valid at large distances from

the dislocation. The following transformation of the Bloch-wave amplitudes is introduced

$$\varphi'(\mathbf{k}_p^l, z) = \varphi''(\mathbf{k}_p^l, z) \exp\left[2\pi i T'' \mathbf{g}_1 \cdot \mathbf{R}(z)\right] , \qquad (3)$$

where $T'' = \sum_g C_g^{l*}(g/g_1)C_g^l$. We neglect the elastic interband scattering ($j \neq l$) in equation (1). By estimating the different terms in equation (1) it is possible to show that this is a reasonable approximation at a distance of a few $s_{lg_1}^{-1}$ from the dislocation (cf. the width of the weak-beam peak $\propto s_{lg_1}^{-1}$ which is caused by interband scattering). For the dominating phonon scattering process ($0 \rightarrow l'$) the following expression is obtained from (A4) and (A5)

$$\varphi''(\mathbf{k}_p^{l'}, t)$$

$$\simeq \int_0^t dz \sum_{\mathbf{hg}} (2\pi^2) C_h^{l'*}[(\mathbf{h}-\mathbf{g}) \cdot \hat{g}_1]C_g^0 \left[\frac{V\hbar}{2NM\zeta_{h-g}^2}\right]^{1/2}$$

$$\times \exp(2\pi i \delta k \cdot z)$$

$$\times \exp\left[2\pi i(T^{00}-T^{l'l'})\mathbf{g}_1 \cdot \mathbf{R}(z)\right]\varphi''(\mathbf{k}_0^0, z) , \quad l' \neq 0', \quad (4)$$

where the wave-vector error δk is equal to $(\mathbf{k}_0^0 + \mathbf{q} - \mathbf{k}_p^{l'})_z$. The Bloch-wave coefficients can be calculated with first-order perturbation theory (Sandström, 1973a). One finds that $C_{lg_1}^l \simeq 1$ and $T^{00} - T'' \simeq -l$. If we assume that $\varphi''(\mathbf{k}_0^0, z)$ is constant through the foil which is well satisfied under weak-beam conditions, we obtain

$$\varphi''(\mathbf{k}_p^{l'}, t) \propto \int_0^t dz \exp 2\pi i(-l'\mathbf{g}_1 \cdot \mathbf{R}(z) + \delta k \cdot z) . \quad (5)$$

As an example we consider the following strain field from a screw dislocation $\mathbf{g}_1 \cdot \mathbf{R} = \mathbf{g}_1 \cdot \mathbf{b}/2\pi$ arctan $[(z-y)/x]$ (see e.g. Hirsch, Howie, Nicholson, Pashley & Whelan, 1965, p. 251) where y is the position of the dislocation and x is the distance from the dislocation in the plane parallel to the foil surface.

Close to the dislocation ($|x| \ll t$) the phase in the integrand changes rapidly by $l'\mathbf{g}_1 \cdot \mathbf{b}\pi$ when going
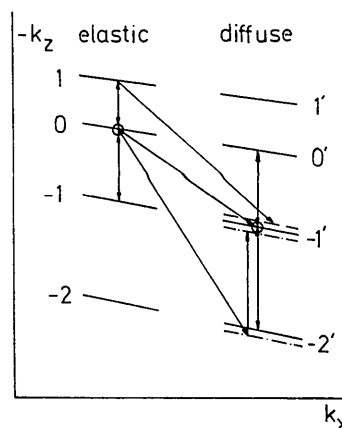

Fig. 3. Dispersion surfaces under weak-beam conditions at 1 MV. The main scattering processes are shown. The figure is not to scale.

from above to below the dislocation. Further away from the dislocation the strain field varies more slowly. The phase has a negligible influence on the integral at a distance of a few foil thicknesses from the dislocation. The small wave-vector errors, $\delta k = n/t$, pick up the slowly varying part of the phase factor as the integral is performed. The intensity of every phonon scattering process thus has a long-range variation.

In a perfect crystal where $R(z) = 0$ almost all the diffuse intensity comes from the wave-vector conserving process ($\delta k = 0$). In fact, from the approximate expression for φ'' given in (5) the contribution from non-conserving processes vanishes altogether. However, in the presence of a defect a finite δk can reduce the variation of the integrand of (5) around the defect and hence increase the value of the integral. Scattering processes with a finite wave-vector error can give a substantial contribution to the intensity.

The total phonon-scattered intensity is obtained by summing over several δk values. For simplicity we assume for the moment being that the phonon occupation number n_q and the angular frequency ω_q are independent of δk. The phonon-scattered intensity is then proportional to

$$I^{ph}_{l'g_1}(t) \propto \frac{1}{t} \sum_n \left| \int_0^t dz \exp\left[2\pi i \left(-l'g_1 \cdot R(z) + \frac{n}{t} \cdot z \right) \right] \right|^2.$$ (6)

The summation over n is performed over the number of available states in the first Brillouin zone. This number is approximately t/a, where a is the lattice parameter. If the summation is extended to infinity, Parseval's relation for complex Fourier series

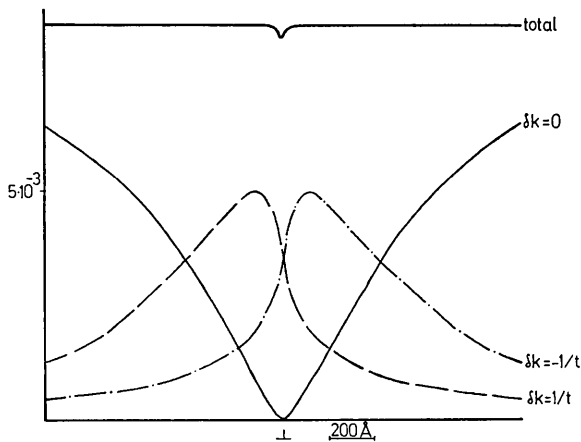$$\frac{1}{t} \int_0^t |g(x)|^2 dx = \sum_{n=-\infty}^{\infty} |C_n|^2$$

Fig. 4. Thermal diffuse intensity around a $\overline{2}20$ spot at 1 MV. A screw dislocation, satisfying $g_1 \cdot b = 1$, is in the middle of a copper foil of thickness 2400 Å. $s_{\overline{2}\overline{2}0} = -0.02$ Å^{-1} ($H = 6.4$). The aperture radius used is 0.2 of a 220 reciprocal-lattice vector and the temperature is 300K in all figures unless otherwise stated.

where

$$C_n = \frac{1}{t} \int_0^t g(x) \exp\left(2\pi i n \frac{x}{t} \right) dx$$ (7)

gives

$$I^{ph}_{l'g_1}(t) \propto \int_0^t dz |\exp 2\pi i [-l'g_1 \cdot R(z)]|^2 = t.$$ (8)

This is exactly the same result as for a perfect crystal which is obtained by putting $R(z) = 0$ in (6). The long-range contrast of the total phonon-scattered intensity thus disappears if an infinite number of phonon modes are available. For a typical foil thickness of 1000 Å the first Brillouin zone has 200 or 300 phonon states in the z direction. Calculations show that this number of states is quite sufficient to yield a negligible long-range contrast.

5. Contrast calculations

Fig. 4 shows the thermal diffuse contrast of a screw dislocation, satisfying $|g_1 \cdot b| = 1$, in the middle of a copper foil at 1 MV. The wave vector conserving process, $\delta k = 0$, gives an intensity which has a minimum at the position of the dislocation. This is in agreement with (5) since $g_1 \cdot R$ has a rapid increase of $\frac{1}{2}$ at the dislocation. Consequently the integrand changes its sign, and if the dislocation is in the middle of the foil, the resulting intensity will vanish. The non-conserving processes $\delta k = \pm 1/t$ have their largest contribution on either side of the dislocation which can also be seen from (5) by rewriting it in the following form

$$\varphi''(\mathbf{k}'_p, t) \propto \int_0^t dz$$
$$\times \exp\left[2\pi i \int_0^z \left(-l'g_1 \cdot \frac{dR(z')}{dz'} + \delta k \right) dz' \right].$$ (9)

where $g_1 \cdot dR/dz = g_1 \cdot b/2\pi \cdot x/[(y-z)^2 + x^2]$ for a screw dislocation. The largest absolute value of the amplitude φ'' is obtained if the integral in the exponential is approximately constant. This occurs when $l'xg_1 \cdot b$ and δk have the same sign. In Fig. 4, l' is $-1'$ and consequently the largest contribution is to the left of the dislocation for $\delta k > 0$ and to the right for $\delta k < 0$.

The total thermal diffuse intensity is obtained by summing the contributions from several wave-vector errors δk. In the calculation presented in Fig. 4 19 δk values have been included. The long-range variation of the total intensity is very weak as anticipated from equation (8). In this case the influence of phonon dispersion is very small, because the most important δk values are small compared to the distance between the dispersion surfaces $|(k^0 - k^{-1'})_z| \simeq |s_{-g_1}|$ of the dominating phonon-scattering process. The minimum in the diffuse intensity close to the dislocation is caused by elastic scattering, preferentially between the primarily excited Bloch waves 0 and 1 in Fig. 3. This contrast is similar to the elastic bright-field contrast which has its dominating contribution from the same process. From a rather complex argument it follows

that the contrast in the diffuse intensity is slightly smaller than in the bright-field intensity. The contrast is much smaller for $|\mathbf{g}_1 . \mathbf{b}| = 1$ than for $|\mathbf{g}_1 . \mathbf{b}| = 2$. An example for $|\mathbf{g}_1 . \mathbf{b}| = 2$ at 1MV is given by Melander & Sandström (1973). The total dislocation contrast in the $-\mathbf{g}_1$ beam including the elastic intensity is shown in Fig. 5. With an aperture radius of 0·2 of a 220 reciprocal-lattice vector the visibility of the peak is 0·1 (the concept of visibility is defined in § 8).

An example of the thermal diffuse contrast at 100 kV is presented in Fig. 6. An edge dislocation with $|\mathbf{g}_1 . \mathbf{b}| = 2$ is in the middle of a Cu foil. The wave-vector conserving process has a maximum close to the dislocation. This can be realized from (5) since $\mathbf{g}_1 . \mathbf{R}$ changes rapidly by one when going from above to below the dislocation. This means that the phase will be the same over almost the whole foil thickness and the intensity of the perfect crystal will almost be obtained. The less rapid variation of the strain field at larger distances from the dislocation results in the minima some 400 Å from the dislocation. The strong elastic scattering in the diffuse state between waves 1′ and 2′ in Fig. 2 gives rise to the minimum on the right-hand side of the dislocation. By summing over ten δk values the total diffuse intensity is obtained. The minimum to the left of the dislocation is caused by elastic scattering, mainly between 0 and 1 and between 1′ and 0′, and the minimum to the right is a result of the process 1′ to 2′. It can be observed that the total intensity to the left of the two minima is more than 10% higher than the intensity to the right. This effect cannot be predicted by the approximate formula (8) which neglects phonon dispersion. $|q_z|$ for the process $0 \rightarrow 1'$ equals $|\delta k + (\mathbf{k}^{1'} - \mathbf{k}^0)_z|$ which means that the most important processes to the left of the dislocation (for which $\delta k < 0$) have smaller $|q_z|$ values than the ones to the right (for which $\delta k > 0$) since $(k^{1'} - k^0)_z$ is positive. A smaller $|q_z|$ implies a larger intensity contribution, as can be observed from (A10). The total diffuse intensity is thus slightly greater to the left of the dislocation than to the right. The total intensity including the elastic part is presented in Fig. 7. The diffuse intensity has a minimum where the elastic intensity has its maximum. The main influence of the diffuse intensity is to increase the background.

6. Top–bottom effect

The variation of the elastic contrast with the depth position of a lattice defect in the foil is usually affected by anomalous absorption. However, under weak-beam conditions the absorption parameters of the Bloch waves which give a significant contribution to the intensity are about the same; so the absorption has little influence on the contrast. All the same, the thermal diffuse contrast can be different from two dislocations, one close to the top surface and the other close to the bottom surface. This can be explained with the help of the dispersion surfaces in Fig. 2.

If the dislocation is situated close to the top surface practically all elastic scattering takes place among the primarily excited states. This means that the processes 0 to 1 and 0 to −1 are dominating. With the dislocation in the middle of the foil the elastic scattering between the diffuse states 1′ to 0′ and 1′ to 2′ is equally important (H is assumed to be about three). The first process gives the same contrast as the scattering from wave 0 to wave 1 and consequently the minimum to the left of the dislocation is insensitive to the dislocation position (cf. Fig. 8). The closer the dislocation is to the bottom surface the larger the influence of the process 1′ to 2′ is on the contrast. This is also clearly seen in Fig. 8 since the minimum to the right of the dislocation is due to the process 1′ to 2′. If H is much bigger than 3 the scattering process 1′ to 2′ is no longer dynamical and consequently the top–bottom effect is small. In the calculations H is smaller than three. It is possible to show with the help of the lattice-bending criterion (Cockayne, Ray & Whelan, 1969) that for H larger than three the minimum will move to the left of the dislocation at least if H is sufficiently different from three.
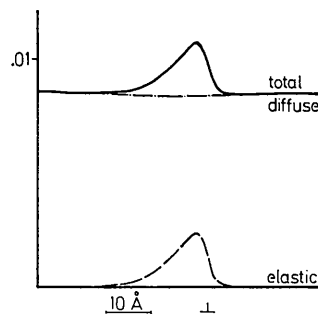
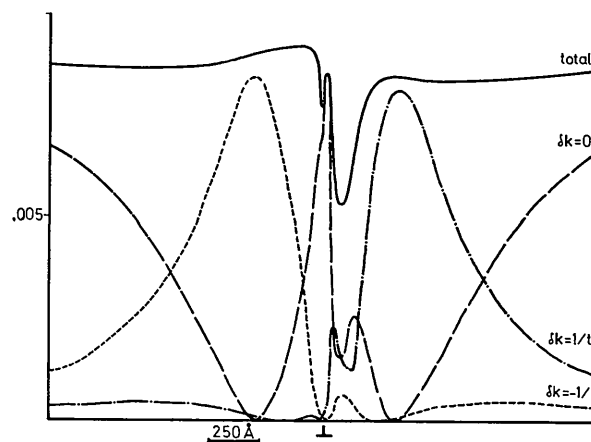Fig. 5. The central region of Fig. 4 including the elastic intensity.

Fig. 6. Thermal diffuse intensity around a 220 spot at 100 kV. An edge dislocation, satisfying $\mathbf{g}_1 . \mathbf{b} = 2$, is in the middle of a copper foil of thickness 675 Å. $s_{220} = 0.02$ Å^{-1} ($H = 2.76$).

The depth of the dislocation also affects the contrast in another way. Calculations show that the intensity contribution from different wave-vector errors δk changes with the depth of the dislocation. If the dislocation is moved from the middle of the foil towards a foil surface the importance of the wave-vector conserving process is increased at the expense of the non-conserving processes. This implies that the asymmetry in the long-range contrast decreases (see § 5).
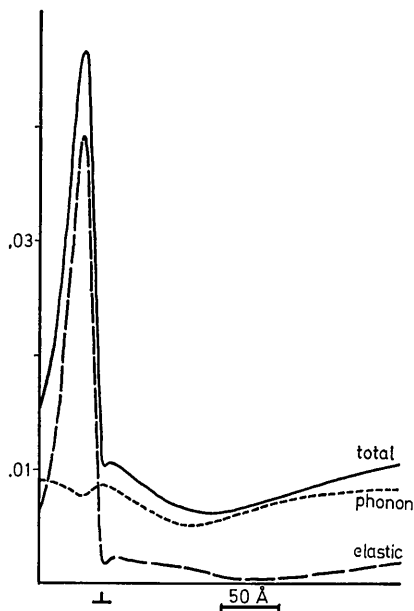

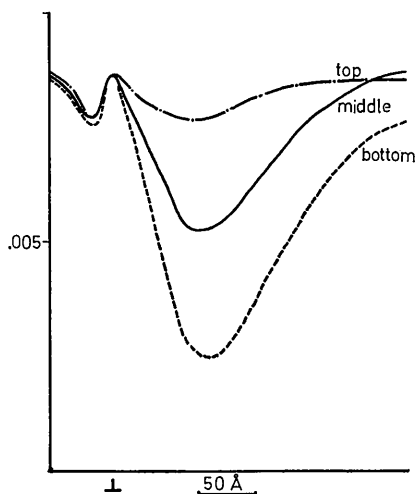Fig. 7. The central region of Fig. 6 including the elastic intensity.

Fig. 8. Top–bottom effect of the thermal diffuse intensity. Same conditions as in Fig. 6. The dislocation is respectively 100 Å from the top surface, in the middle of the foil and 100 Å from the bottom surface.

7. Diffuse intensity in perfect crystals

7.1. Thickness and aperture dependence of the thermal diffuse intensity

If the crystal is oriented between two higher-order Bragg positions it is possible to obtain a simple expression for the thermal diffuse intensity around the $l\mathbf{g}_1$ spot in a perfect crystal. In a perfect crystal the first sum in equation (A4) vanishes and for the prescribed diffraction conditions in the second sum only the dominating term is kept ($i=0$, $\mathbf{g}=0$ and $\mathbf{h}=l'\mathbf{g}_1$). Thus only the scattering process from 0 to l' is considered. As was shown in § 4 only the amplitudes for $\delta k=0$ are important in a perfect crystal. After absorption is introduced equation (A4) takes the following form after the application of equation (A5)

$$\varphi'(\mathbf{k}_p^{l'},t) \simeq 4\pi^2 \frac{l'g_1}{\xi_{l'g_1}} \left[\frac{\hbar V}{2NM}\right]^{1/2}$$

$$\times \frac{\exp\left[-\tfrac{1}{2}(\mu^0-\mu^{l'})t\right]-1}{\mu^0-\mu^{l'}} \varphi(\mathbf{k}_0^0,0). \quad (10)$$

By making similar approximations in equation (A7) one finds that only one term in the sums over l and q_z must be kept in the first summation. The second term in (A7) is much smaller than the first one and is neglected:

$$I^{ph}_{l'g_1}(t) \simeq \frac{1}{t} |\varphi'(\mathbf{k}_p^{l'},t)|^2 \exp\left(-\mu^l t\right) A(q_z, q_{\parallel}^{max}). \quad (11)$$

Recalling that $\mu^0-\mu^l$ is small, one observes easily that the intensity (11) has a maximum at $t\simeq 1/\mu^l \simeq 1/\mu^0$. Equations (10) and (11) have been used to calculate the diffuse intensity around a 220 reflexion. The intensity as a function of foil thickness is presented in Fig. 9 for Al, Cu and Au at 1 MV and for Cu at 100 kV. Weak-beam images are usually obtained for foil thicknesses between 200 and 800 Å in Cu at 100 kV (Stobbs & Sworn, 1971). The calculations show that the thermal diffuse intensity increases by a factor of 1·6 over this region. The validity of the present single-phonon scattering theory for thicker foils has been investigated by calculating the intensity contribution from electrons that have been scattered twice by phonons. These electrons have first been scattered outside the aperture and then into the aperture. In the calculation the rigid-ion model has been used with an Einstein model. The details of the calculation are rather lengthy and are not presented here. For Al, Cu and Au we have found that the double-scattering intensity I_2 relates to the single-scattering intensity I_1 as

$$I_2/I_1 = 0\cdot2\mu t. \quad (12)$$

Thus, at the maximum thickness presented for every curve in Fig. 9 the thermal diffuse intensity is underestimated by about 30%.

From (10) and (11) we observe that $I^{ph}_{l'g_1}(t)$ is proportional to $(l'g_1/\xi_{l'g_1})^2$. One can check that this implies that the diffuse intensity for the considered metals

is greater in a 111 reflexion than in a 220 reflexion for the same excitation error. The aperture integral $A(q_z, q_{\parallel}^{max})$ increases with decreasing s_{lg_1} and thus also the diffuse intensity increases with decreasing s_{lg_1}. In Fig. 10 the variation of the thermal diffuse intensity with aperture radius is shown for Cu. The diffuse intensity is peaked around the reciprocal-lattice points, so quite a small aperture is required to reduce the intensity significantly.

7.2. Contaminating layers

We will also discuss the diffuse background intensity from contaminating carbon layers which are almost always present on the foil surfaces. An amorphous layer can scatter an incoming electron elastically or inelastically into the aperture around the lg_1 spot. This intensity can be estimated with the help of the theories of Lenz (1954) and Burge & Smith (1962). An amorphous carbon layer of thickness D Å thus gives an intensity of $1 \cdot 10^{-5} D$ around the 220 spot in copper at 100 kV when the aperture radius is 0·2 of a 220 reciprocal-lattice vector. At 1 MV the intensity is smaller by a factor of $(v_{1\ MV}/v_{100\ kV})^2 \simeq 3$, where v is the relativistic electron velocity. For small radii the intensity is approximately proportional to the aperture radius squared. If the contaminating layers are not essentially thicker than 100 Å together, their contribution to the background intensity $1 \cdot 10^{-3}$ at 100 kV is significantly smaller than the thermal diffuse intensity for the foil thicknesses that are usually used in weak-beam microscopy.

8. Visibility

The visibility, as given by an elastic calculation, can be significantly reduced when the thermal diffuse intensity is taken into account. The visibility is defined as $(I_{max} - I_{min})/(I_{max} + I_{min})$ where I_{max} and I_{min} are the maximum and minimum intensities of a contrast profile. The elastic intensity has an oscillating dependence on the depth of the dislocation and the foil thickness, the period of the oscillations being $s_{lg_1}^{-1}$ (Sandström, 1973b). To obtain a measure of the visibility an average over the oscillating terms of the intensity is taken. We use the approximate expressions for the intensity of the weak-beam peaks given by Sandström (1973a) which are based on a simplified strain field and a kinematical approximation. After some algebra the average peak intensity emerges as

$$I_{lg_1}^{peak}(t) \simeq \left[\frac{K}{\xi_{lg_1} \cdot g_1^2 \cdot l(H-l)}\right]^2 [2 + \pi^2(\mathbf{g}_1 \cdot \mathbf{b})^2]$$
$$\times \exp(-\mu t), \quad (13)$$

where K is the wave vector of the incident electrons. The elastic background intensity close to the weak-beam peak is obtained from (13) if $\pi^2(\mathbf{g}_1 \cdot \mathbf{b})^2$ is replaced by $\frac{4}{9}(\mathbf{g}_1 \cdot \mathbf{b})^2$. The thermal diffuse intensity is approximated by the expression for the perfect crys-

tal (11). The influence of contaminating layers is neglected. The visibility B can now be written as

$$B \simeq \left\{\left(\frac{1}{2s_{lg_1}}\right)^2 \cdot (\pi^2 - \tfrac{4}{9}) \cdot (\mathbf{g}_1 \cdot \mathbf{b})^2\right\} \Big/ \left\{\left(\frac{1}{2s_{lg_1}}\right)^2 [4 + (\pi^2 + \tfrac{4}{9})\right.$$
$$\left.\times (\mathbf{g}_1 \cdot \mathbf{b})^2] + 2|2\pi^2 lg_1\left(\frac{hV}{2NM}\right)^{1/2} l^2 t A(q_z, q_{\parallel}^{max})\right\}. \quad (14)$$

The derivation of (13) is very approximate but comparisons with many-beam calculations indicate that it overestimates the visibility only by about 20%. We notice that B is independent of the accelerating voltage. Fig. 11 shows the visibility for a dislocation as a function of foil thickness for aluminum, copper and gold. For aluminum the visibility is presented for two different excitation errors. The dislocation is observed under the diffraction condition $\mathbf{g}_1 \cdot \mathbf{b} = 2$. The visibility is about the same in Al, Cu and Au for a particular foil thickness and excitation error, but it is much lower in the lighter metals for a foil of thickness λ_p ($\lambda_p \simeq 580$ Å for Au, 2300 Å for Cu and 10000 Å for Al at 1 MV, Hall & Hirsch, 1965). The visibility is presented for foil thicknesses up to the mean free path for phonon scattering λ_p at 1 MV. It must be remembered, how-
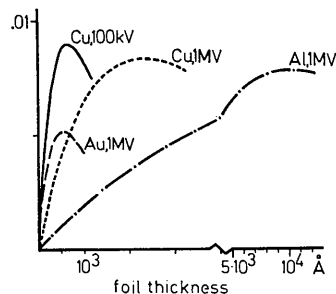

Fig. 9. Thermal diffuse intensity (220) from a perfect crystal for Al, Cu and Au at 1MV and for Cu at 100 kV. The aperture radius is 0·2 of a 220 reciprocal-lattice vector in aluminum. The scale for the foil thickness is changed at 4000 Å.
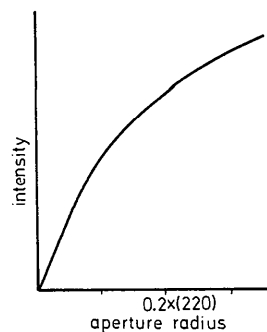

Fig. 10. Thermal diffuse intensity (220) *versus* aperture radius for copper foil. $|s_{220}| = 0·02$ Å^{-1}. The form of the curve is the same for every foil thickness.

ever, that the theory is not applicable for foil thicknesses much larger than λ_p which means that the diagram is not valid along the whole abscissa at lower voltages since λ_p is proportional to v^2.

If the excitation error is reduced the elastic intensity increases more rapidly than the thermal diffuse intensity and thus the visibility increases. This is seen in Fig. 11 for aluminum by comparing the curves for $s_{220} = 0.02$ Å^{-1} and $s_{220} = 0.01$ Å^{-1}. The resolution decreases simultaneously, however, because the half width of the weak-beam peak is proportional to $|s_{lg_1}|^{-1}$ (de Ridder & Amelinckx, 1971). The visibility for a dislocation as function of aperture radius is presented in Fig. 12. An aperture smaller than 0·15 of a 220 recip-
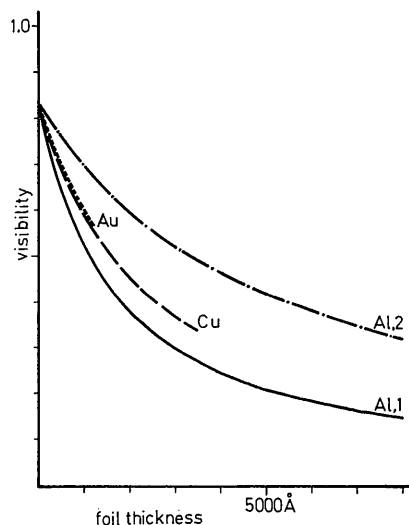
rocal-lattice vector is required to increase the visibility significantly. However, such a small aperture will on the other hand impair the resolution according to the fundamental diffraction limit. To maximize the visibility g_1 should of course be parallel to b since the elastic peak intensity is proportional to $|g_1 . b|^2$.

The thermal diffuse intensity decreases if the temperature is lowered. Calculations under the same conditions as in Fig. 12, and using an aperture radius of 0·2 of a 220 reciprocal-lattice vector, show an increase in the visibility from 0·3 at 300 K to 0·5 at 80 K and to 0·6 at 0 K.

In contrast to the visibility, the elastic peak intensity depends on the accelerating voltage as can be seen from equation (13). If we use the same excitation error at all voltages the peak intensity is proportional to

$$I^{peak}_{lg_1} \propto \exp\left[-\mu_{100} . \left(\frac{v_{100}}{v}\right)^2 . t\right] . \left(\frac{v_{100}}{v}\right)^2, \quad (15)$$

where the relativistic corrections of μ and ξ_{g_1} have been included. For a certain foil thickness the maximum intensity is obtained for the accelerating voltage

$$E = \frac{m_0 c^2}{e}\left[\frac{1}{\sqrt{1 - \left(\frac{v_{100}}{c}\right)^2 \mu_{100} . t}} - 1\right] \text{ if } t < \left(\frac{c}{v_{100}}\right)^2 \mu_{100} .$$

The maximum intensity is proportional to t^{-1}. For foils thicker than $(c/v_{100})^2/\mu_{100}$ the maximum voltage should be used to maximize intensity.

Fig. 11. Visibility in the 220 image of a dislocation satisfying $|g_1 . b| = 2$ for Al (denoted Al, 1), Cu and Au with an excitation error of 0·02 Å^{-1} and for Al (denoted Al, 2) with $s_{220} = 0.01$ Å^{-1}.
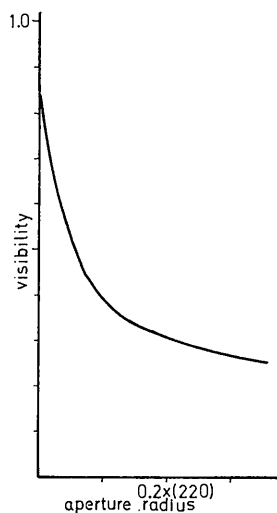

Fig. 12. Visibility in the 220 image of a dislocation satisfying $|g_1 . b| = 2$ in a 3000 Å thick aluminum foil. $|s_{220}| = 0.02$ Å^{-1}.

Conclusions

1. In weak-beam images the thermal diffuse and elastic intensities are comparable in magnitude for foil thicknesses of the order of the mean free path for electron–phonon scattering.

2. Phonon scattering processes where the wave vector is not conserved in the direction of the foil normal play an important role in the contrast formation.

3. The thermal diffuse intensity has a minimum at the position of the weak-beam peak in a similar way to in the elastic bright-field contrast.

4. If the total thickness of contaminating carbon layers is approximately 100 Å, the diffuse intensity from them is much smaller than the thermal diffuse intensity for foil thicknesses conventionally used in weak-beam investigations.

5. The visibility in weak-beam images is independent of the accelerating voltage. For a certain foil thickness and excitation error the visibility is comparable for different metals.

APPENDIX

In the deformable-ion model the interaction between the incident electron and the lattice is given by

$$V(r) = V_p[r - R(r) - u(r)] .$$

V_p is the potential of the perfect crystal and $\mathbf{u}(\mathbf{r})$ are the atom displacements due to lattice vibrations. The Hamiltonian $H(\mathbf{r})$ is obtained by expanding $V(\mathbf{r})$ in a Taylor series in $\mathbf{u}(\mathbf{r})$ and keeping first-order terms in $\mathbf{u}(\mathbf{r})$. The influence of the strain field on the phonon modes has been neglected and the perfect crystal expansion of $\mathbf{u}(\mathbf{r})$ has been used (see *e.g.* Pines, 1963). The Hamiltonian for the electron–phonon system in the deformable ion model can be written as

$$H(\mathbf{r}) = -\frac{\hbar^2}{2m}\nabla^2 - \sum_{\mathbf{g}} V_{\mathbf{g}} \exp\{2\pi i\mathbf{g}[\mathbf{r}-\mathbf{R}(\mathbf{r})]\}$$

$$-\sum_{\mathbf{g}\mathbf{q}\lambda} V_{\mathbf{g}} \exp\{2\pi i\mathbf{g}[\mathbf{r}-\mathbf{R}(\mathbf{r})]\}\,(-2\pi i)\,(\boldsymbol{\varepsilon}_{\mathbf{q}\lambda}\cdot\mathbf{g})$$

$$\times\left(\frac{\hbar}{2NM\omega_{\mathbf{q}\lambda}}\right)^{1/2}\exp(2\pi i\mathbf{q}\cdot\mathbf{r})\,(a_{\mathbf{q}\lambda}+a_{-\mathbf{q}\lambda}^+)$$

$$+\sum_{\mathbf{q}\lambda}\hbar\omega_{\mathbf{q}\lambda}(a_{\mathbf{q}\lambda}^+ a_{\mathbf{q}\lambda}+\tfrac{1}{2})\,. \tag{A1}$$

The potential parameters $V_{\mathbf{g}}$ include Debye–Waller factors. $a_{\mathbf{q}\lambda}$ is the annihilation operator of the phonon mode $(\mathbf{q},\lambda)$. The phonon wave vectors $\mathbf{q}$ are restricted to the first Brillouin zone. We adopt the column approximation and assume that the electron–phonon state can be written (z axis parallel to the foil normal)

$$\psi(\mathbf{r}) = \sum_{Q,\,\mathbf{k}_Q^j} \varphi(\mathbf{k}_Q^j,z)b(\mathbf{k}_Q^j,\mathbf{r})|Q\rangle\,, \tag{A2}$$

where $|Q\rangle = |n_{\mathbf{q}_1\lambda_1}\ldots n_{\mathbf{q}_n\lambda_n}\ldots\rangle$. The Bloch wave $b(\mathbf{k}_Q^j,\mathbf{r})$ is given by (Wilkens, 1964)

$$b(\mathbf{k}_Q^j,\mathbf{r}) = \sum_{\mathbf{g}} C_{\mathbf{g}}^j \exp 2\pi i\{\mathbf{k}_Q^j\cdot\mathbf{r}+\mathbf{g}[\mathbf{r}-\mathbf{R}(z)]\}\,. \tag{A3}$$

The summation in (A2) is taken over all phonon states Q and over all Bloch states such that the total energy is constant.

From the Schrödinger equation we obtain the Bloch-wave amplitudes by performing

$$\int\int_{-\infty}^{\infty}\mathrm{d}x\mathrm{d}y\,b^*(\mathbf{k}_{p\pm}^l,\mathbf{r})\langle p^\pm|\,,$$

where $|p^\pm\rangle = |n_{\mathbf{q}_1\lambda_1}^0\ldots(n_{\mp\mathbf{q}_n\lambda_n}^0\pm 1)\ldots\rangle$. The upper signs correspond to creation of one phonon $(-\mathbf{q}_n,\lambda_n)$ and the lower signs to annihilation of one phonon. We neglect multiple-phonon scattering as well as second-order derivatives of $\mathbf{R}(z)$ and $\varphi(\mathbf{k}^i,z)$ and obtain for creation of phonons

$$\frac{\mathrm{d}}{\mathrm{d}z}\varphi(\mathbf{k}_{p+}^l,z)$$

$$=2\pi i\sum_{\mathbf{g}j}C_{\mathbf{g}}^{l*}\left(\mathbf{g}\cdot\frac{\mathrm{d}\mathbf{R}}{\mathrm{d}z}\right)C_{\mathbf{g}}^j\exp[2\pi i(\mathbf{k}_{p+}^j$$

$$-\mathbf{k}_{p+}^l)_z\cdot z]\varphi(\mathbf{k}_{p+}^j,z)$$

$$+2\pi^2\sum_{\mathbf{g}\mathbf{h}i}C_{\mathbf{h}}^{l*}\frac{1}{\xi_{\mathbf{h}-\mathbf{g}}}C_{\mathbf{g}}^i[\boldsymbol{\varepsilon}_{\mathbf{q}\lambda}\cdot(\mathbf{h}-\mathbf{g})]\left[\frac{\hbar(n_{-\mathbf{q}\lambda}^0+1)}{2NM\omega_{\mathbf{q}\lambda}}\right]^{1/2}$$

$$\times\exp[2\pi i(\mathbf{k}_0^i+\mathbf{q}-\mathbf{k}_{p+}^l)_z\cdot z]\varphi(\mathbf{k}_0^i,z)\,. \tag{A4}$$

For phonon annihilation (1) is identical to (A4) except that $n_{-\mathbf{q}\lambda}^0+1$ has to be replaced by $n_{\mathbf{q}\lambda}^0$. Absorption is introduced by letting $\mathbf{k}_p^l\to\mathbf{k}_p^l+i\mu^l/4\pi$, where μ^l is the absorption coefficient for Bloch wave l. Through the following transformations the equations (1) and (A4) become independent of polarization index and whether a phonon is created or annihilated:

$$\varphi(\mathbf{k}_{p+}^l,z) = (\boldsymbol{\varepsilon}_{\mathbf{q}\lambda}\cdot\hat{\mathbf{g}}_1)\left[\frac{n_{-\mathbf{q}\lambda+1}^0}{\omega_{\mathbf{q}\lambda}\cdot V}\right]^{1/2}\varphi'(\mathbf{k}_p^l,z)\,,$$

$$\varphi(\mathbf{k}_{p-}^l,z) = (\boldsymbol{\varepsilon}_{\mathbf{q}\lambda}\cdot\hat{\mathbf{g}}_1)\left[\frac{n_{\mathbf{q}\lambda}^0}{\omega_{\mathbf{q}\lambda}\cdot V}\right]^{1/2}\varphi'(\mathbf{k}_p^l,z)\,, \tag{A5}$$

where V is the crystal volume. Only systematic reciprocal-lattice vectors are taken into account. $\hat{\mathbf{g}}_1$ is $\mathbf{g}_1/g_1$ where $\mathbf{g}_1$ is the first-order reciprocal-lattice vector of the systematic row. Thus for every phonon wave vector only one equation has to be solved. The Debye model is used to describe the phonon dispersion relations. The summation over the polarization indices can now be performed and phonon creation and annihilation can be taken together. The factor depending on q takes the following form

$$\sum_\lambda(\boldsymbol{\varepsilon}_{\mathbf{q}\lambda}\cdot\hat{\mathbf{g}}_1)^2\frac{2n_q+1}{\omega_q} = \frac{2n_q+1}{\omega_q} \tag{A6}$$

where the temperature average has been taken. $n_q = 1/[\exp(hv_D q/k_B T)-1]$ where k_B is Boltzmann's constant, T the temperature, and the Debye velocity $v_D = k_B\theta_D\left(\frac{4\pi}{3}\frac{V}{N}\right)^{1/3}/h$. The numerical values of the Debye temperature θ_D in *International Tables for X-ray Crystallography* (1962) have been used.

If the transformed amplitudes (A5) are approximated to be independent of q_x and q_y the thermal diffuse intensity (2) accepted by the aperture around $\mathbf{g}$ can be written as

$$I_{\mathbf{g}}^{\mathrm{ph}}(t) \simeq \sum_{q_z}\frac{1}{t}\Big\{\sum_l|\varphi'(\mathbf{k}_p^l,t)C_{\mathbf{g}}^l|^2\exp(-\mu^l t)A(q_z,q_{\parallel}^{\max})$$

$$+\sum_{l_1\neq l_2}2\mathrm{Re}[\varphi'^*(\mathbf{k}_p^{l_1},t)C_{\mathbf{g}}^{l_1*}\varphi'(\mathbf{k}_p^{l_2},t)C_{\mathbf{g}}^{l_2}$$

$$\times\exp[2\pi i(\mathbf{k}_0^{l_2}-\mathbf{k}_0^{l_1})_z t]]$$

$$\times\exp[-\tfrac{1}{2}(\mu^{l_1}+\mu^{l_2})t]B(q_z,q_{\parallel}^{\max},t)\Big\} \tag{A7}$$

$$A(q_z,q_{\parallel}^{\max}) = \int_0^{q_{\parallel}^{\max}}2\pi q_{\parallel}\,\mathrm{d}q_{\parallel}\frac{2n_q+1}{v_D\cdot q} \tag{A8}$$

$$B(q_z,q_{\parallel}^{\max},t) = \int_0^{q_{\parallel}^{\max}}q_{\parallel}\,\mathrm{d}q_{\parallel}\int_0^{2\pi}\mathrm{d}\theta\frac{2n_q+1}{v_D\cdot q}$$

$$\times\exp[2\pi i(\mathbf{k}_p^{l_2}-\mathbf{k}_0^{l_2}-\mathbf{k}_p^{l_1}+\mathbf{k}_0^{l_1})_z\cdot t]\,. \tag{A9}$$

All states included in the summation over l, l_1 and l_2 have been scattered from the initially excited Bloch waves by the same phonon. t is the foil thickness and

$q_\parallel$ is the component of the phonon wave vector $\mathbf{q}$ in the plane of the aperture. $q_\parallel^{max}$ is the radius of the aperture and $q^2 = q_z^2 + q_\parallel^2$. θ is the angle between $\mathbf{q}_\parallel$ and the direction of the systematic row $\hat{\mathbf{g}}_1$. We introduce the following approximations in (A8): q is put equal to $q_\parallel$ and the lower integration limit is replaced by $|q_z|$. The integral can now be solved analytically as

$$A(q_z, g_\parallel^{max}) \simeq \frac{2\pi}{v_D} \left\{ |q_z| - q_\parallel^{max} + \frac{2k_B \cdot T}{\hbar v_D} \right.$$
$$\left. \times \ln \left[\frac{\exp\left(\frac{\hbar v_D}{k_B \cdot T} q_\parallel^{max}\right) - 1}{\exp\left(\frac{\hbar v_D}{k_B \cdot T} |q_z|\right) - 1} \right] \right\}. \quad (A10)$$

The approximation is very good if $q_\parallel^{max} \gg |q_z|$. (A10) is found to agree within one per cent with accurate numerical evaluations of (A8) if $q_\parallel^{max} \gtrsim 0.15 \ \text{Å}^{-1}$ and $|q_z| = 0.02 \ \text{Å}^{-1}$.

The integral over θ in (A9) is evaluated by approximating $(k_0^l)_z^2 \simeq K^2 - (H/2 - l)^2 g_1^2$ and $(k_p^l)_z^2 \simeq K^2 - (H/2 - l + q_x/g_1)^2 g_1^2$ where K is the wave vector of the incident electron and the Ewald sphere intersects the systematic row at $H \cdot \mathbf{g}_1$. Thus $(\mathbf{k}_p^{l2} - \mathbf{k}_0^{l2} - \mathbf{k}_p^{l1} + \mathbf{k}_0^{l1})_z \simeq (l_2 - l_1) g_1 q_\parallel \cos\theta/K$ and

$$B(q_z, q_\parallel^{max}, t) \simeq \int_0^{q_\parallel^{max}} 2\pi q_\parallel \, dq_\parallel \frac{2n_q + 1}{v_D q}$$
$$\times J_0(2\pi(l_2 - l_1) g_1 q_\parallel t/K), \quad (A11)$$

where J_0 is the zeroth-order Bessel function. J_0 causes the t-oscillating terms of the intensity to be damped out for large apertures.

References

BURGE, R. E. & SMITH, G. H. (1962). *Proc. Phys. Soc.* **79**, 673–690.

CASTAING, R., HÉNOC, P., HENRY, L. & NATTA, M. (1967). *C.R. Acad. Sci. Paris B*, **265**, 1293–1296.

COCKAYNE, D. J. H. (1972). *Z. Naturforsch.* **27a**, 452–460.

COCKAYNE, D. J. H., RAY, I. L. F. & WHELAN, M. J. (1969). *Phil. Mag.* **20**, 1265–1275.

GJÖNNES, J. (1966). *Acta Cryst.* **20**, 240–249.

HALL, C. R. & HIRSCH, P. B. (1965). *Proc. Roy. Soc.* A**286**, 158–177.

HIRSCH, P. B., HOWIE, A., NICHOLSON, R. B., PASHLEY, D. W. & WHELAN, M. J. (1965). *Electron Microscopy of Thin Crystals*. London: Butterworth.

HOWIE, A. (1963). *Proc. Roy. Soc.* A**271**, 268–287.

HÖIER, R. (1972). *Proc. 5th European Congress on Electron Microscopy, Manchester*, pp. 444–445.

International Tables for X-ray Crystallography (1962). Vol. III. Birmingham: Kynoch Press.

KAMIYA, Y. & NAKAI, Y. (1971). *J. Phys. Soc. Japan.* **31**, 195–203.

LENZ, F. (1954). *Z. Naturforsch.* **9a**, 185–204.

MELANDER, A. & SANDSTRÖM, R. (1973). *High Voltage Electron Microscopy*, Proc. Third Int. Conf., Edited by P. R. SWANN, C. J. HUMPHREYS and M. J. GORINGE, pp. 27–31. London and New York: Academic Press.

NATTA, M. (1968). *J. Phys. Radium*, **29**, 337–344.

PINES, D. (1963). *Elementary Excitations in Solids*. New York: Benjamin.

RIDDER, R. DE & AMELINCKX, S. (1971). *Phys. Stat. Sol.* **43**, 541–550.

SANDSTRÖM, R. (1973a). *Phys. Stat. Sol.* (a), **18**, 639–649.

SANDSTRÖM, R. (1973b). *Phys. Stat. Sol.* (a), **19**, 83–91.

STOBBS, W. M. & SWORN, C. H. (1971). *Phil. Mag.* **24**, 1365–1381.

TAKAGI, S. (1958). *J. Phys. Soc. Japan*, **13**, 278–296.

WILKENS, M. (1964). *Phys. Stat. Sol.* **6**, 939–956.